SAND75-0051

Unlimited Release

Thermal Model for Solid Rocket Propellant Fires

D. O. Lee, H. C. Hardee, and A. B. Donaldson

Prepared by Sandia Laboratories, Albuquerque, New Mexico 87115 and Livermore, California 94550 for the United States Energy Research and Development Administration under Contract AT(29–1)-789

Printed May 1975

Sandia Laboratories

SF 2900 Q(7-73)

When printing a copy of any digitized SAND Report, you are required to update the markings to current standards.

Issued by Sandia Laboratories, operated for the United States Energy Research and Development Administration by Sandia Corporation.

NOTICE

This report was prepared as an account of work sponsored by the United States Government. Neither the United States nor the United States Energy Research and Development Administration, nor any of their employees, nor any of their contractors, subcontractors, or their employees, makes any warranty, express or implied, or assumes any legal liability or responsibility for the accuracy, completeness or usefulness of any information, apparatus, product or process disclosed, or represents that its use would not infringe privately owned rights.

SAND75-0051
Unlimited Release
Printed May 1975

THERMAL MODEL FOR SOLID ROCKET PROPELLANT FIRES

D. O. Lee and H. C. Hardee
Heat Transfer and Fluid Mechanics Division 1543
A. B. Donaldson
Initiating and Pyrotechnic Component Division 2515
Sandia Laboratories
Albuquerque, New Mexico 87115

ABSTRACT

An analytical model of the heat flux from burning solid rocket propellants in an abort situation is developed. The results of this model are compared with test data from several propellants. The tests indicate that the model provides an upper bound on the heat flux for a given propellant.

CONTENTS

	Page
Introduction	5
Model Development	5
Linear Regression (Burn) on a Flat Surface	5
Burn in a Cylindrical Annulus	9
Discussion of Other Assumptions	10
Determination of Adiabatic Flame Temperature	11
Burn Tests and Comparison of Results with Model	12
Test Setup	12
Annular Burn	16
Flat-Surface Burn	16
Discussion of the Discrepancy in Adiabatic Flame Temperatures	19
Conclusions	20
Recommendations	21
References	21
Appendix	22

ACKNOWLEDGMENT

The authors thank Mrs. Mina Carnicom, who performed the chemical equilibrium calculations.

THERMAL MODEL FOR SOLID ROCKET PROPELLANT FIRES

Introduction

Thermal radiation from fireballs was first analyzed by Van Nice and Carpenter[1] for fireballs resulting from aborts of liquid-fueled rockets. In 1966, a fireball model,[2] based on some of the analytical results of Ref. 1, was developed for liquid-fueled rockets. In 1971, this model was revised and generalized by Bader et al.[3] In 1973 the models were extended further by Hardee and Lee[4] to include fireballs resulting from the rupture of railroad tank cars carrying liquified petroleum gas.

When a solid-propellant rocket fails to lift off or is aborted on the pad, an explosion occurs which results in a pseudo-fireball and in fragmentation of the solid-propellant motor. The fireballs last only moments, and hence, in contrast to the liquid-propellant fireballs described in Refs. 1-3, do not present much hazard. However, fragments of the solid-propellant motor, some of which will be burning, are scattered around the pad, creating a potential hazard to any hardware in the vicinity. Since some of this hardware may contain radioactive material, an understanding of the thermal environment caused by burning propellants is desirable so that the thermal response of this hardware may be predicted.

In this paper, an analytical model is developed and compared with the results of burn tests conducted on several types of solid propellants. The available test data tend to verify the model; however, certain assumptions used in the model require refinement.

Model Development

Linear Regression (Burn) on a Flat Surface

In the model it is assumed that the burning surface of the propellant is at the atmospheric-pressure adiabatic flame temperature. In an actual situation, the surface temperature of the propellant is generally limited to that of a phase transition. The maximum temperature occurs in the gas phase at a point a few hundred microns away from the burning surface. As the flame travels away from the surface it is considered an opaque radiating gas that cools as it loses energy to the surroundings.

If it is assumed that a steady state exists after the propellant burn is established, then the following energy balance, where no mass accumulation occurs, can be written for a control volume in the flame plume shown in Fig. 1:

$$Q_{loss} = -\dot{m}dh \tag{1}$$

or

$$\epsilon\sigma A_s \theta^4 = \dot{m}C_p d\theta \tag{2}$$

where A_s is the lateral surface area of the control volume, $\dot{m}$ is the mass-flow rate through the volume, ϵ is the apparent flame emissivity, and C_p is the average specific heat of the flame along the length of the plume. Because the enthalpy was written proportional to the temperature, it is assumed that no further chemical reaction occurs after initial combustion of the propellant. It is also assumed in Eq. 2 that the surroundings are always cooler than the flame plume, so that radiation in the opposite direction can be neglected. Then

$$-\frac{d\theta}{\theta^4} = \frac{4\epsilon\sigma}{\rho_f V C_p D} d\xi \ , \tag{3}$$

where ρ_f is flame density and V is the velocity of the flame through the control volume. The diameter of the flame, D, is assumed constant and equal to the diameter of the propellant sample. It has been found, when linear regression was experimentally produced, that the flame diameter is only slightly larger than the propellant diameter.

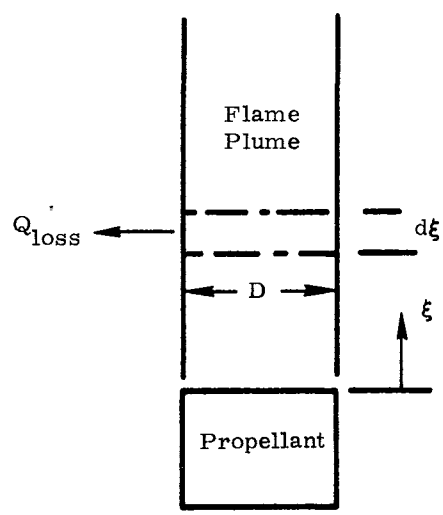

Figure 1. Schematic of Flame Plume

In the absence of air entrainment, continuity yields

$$\rho r_b = \rho_f V \tag{4}$$

where ρ is propellant density and r_b is burn rate. Combining Eqs. 3 and 4 and integrating along the flame-plume length yields

$$-\int_{T_o}^{T} \frac{d\theta}{\theta^4} = \frac{4\epsilon\sigma}{\rho r_b C_p D} \int_o^X d\xi \tag{5}$$

The solution of Eq. 5 yields

$$T = T_o \left[\frac{1}{1 + 12\, P\epsilon \frac{X}{D}} \right]^{1/3} \tag{6}$$

where T_o is the adiabatic flame temperature and P, the propellant number, is defined as

$$P = \frac{\sigma T_o^3}{\rho r_b C_p} \quad . \tag{7}$$

If the apparent emissivity at the surface of the flame is the same as that inside, the heat flux received by a body in the flame would be

$$q = \sigma\epsilon T^4 \quad . \tag{8}$$

Combining Eqs. 6 and 8 yields

$$q = \sigma\epsilon T_o^4 \left[\frac{1}{1 + 12\, P\epsilon \frac{X}{D}} \right]^{4/3} \tag{9}$$

A low emissivity value will reduce the heat flux but at the same time will increase the temperature in the plume. This implies that there is an ϵ that would give the highest heat flux. This can be obtained by maximizing q with respect to ϵ. Hence the following solution is obtained:

$$\frac{3}{4}\left(1 + 12\, P \frac{X}{D}\, \epsilon\right) = 12\epsilon P \frac{X}{D} \tag{10}$$

or

$$\epsilon = \left[4P\frac{X}{D}\right]^{-1}$$

with (11)

$$\frac{X}{D} \geq (4P)^{-1} \quad ,$$

since the following condition must always be satisfied:

$$\epsilon \leq 1 \quad .$$

The maximum heat flux is then:

$$q_{max} = \frac{\sigma T_o^4}{(4)^{7/3}\, P\frac{X}{D}} \quad , \tag{12}$$

for

$$\frac{X}{D} \geq \frac{1}{4P} \quad .$$

For

$\frac{X}{D} < \frac{1}{4P}$ the maximum heat flux occurs when $\epsilon = 1$; hence

$$q_{max} = \frac{\sigma T_o^4}{\left[1 + 12\, P\frac{X}{D}\right]^{4/3}} \tag{13}$$

for

$$\frac{X}{D} \leq \frac{1}{4P}$$

Equations 12 and 13 are the basic thermal-model equations for the heat flux to an object surrounded by a solid-propellant flame.

Burn in a Cylindrical Annulus

Although an annular burn does not normally occur as a result of an accident, experimental reasons (discussed later) require that a model be developed for this case. Only the propellant in the hole is burning, as shown in Fig. 2.

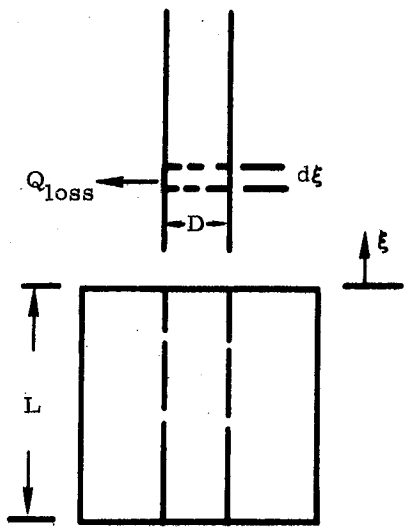

Figure 2. Schematic of an Annular Burn

In a treatment similar to that of the flat-surface burn, an energy balance on the control volume yields

$$-\frac{d\theta}{\theta^4} = \frac{4\epsilon\sigma}{\rho_f V C_p D}\, d\xi \quad . \tag{3}$$

Continuity yields

$$\rho_f V = 4\rho r_b \frac{L}{D} \quad . \tag{14}$$

The solution of Eqs. (3) and (14) yields

$$T = T_o \left[\frac{1}{1 + 3P\epsilon\frac{X}{L}}\right]^{1/3} \quad . \tag{15}$$

Note that the solution is independent of D.

The equations for maximum heat flux are

$$q_{max} = \frac{\sigma T_o^4}{(4)^{4/3} P \frac{X}{L}}$$

for (16)

$$\frac{X}{L} \geq \frac{1}{P}$$

and

$$q_{max} = \frac{\sigma T_o^4}{\left[1 + 3P\frac{X}{L}\right]^{4/3}}$$

for (17)

$$\frac{X}{L} \leq \frac{1}{P} \quad .$$

Discussion of Other Assumptions

Heat transfer by deposition of combustion products on a body in a fire is not treated here, because deposition would depend upon the geometry, temperature, and surface conditions of the body and the local flow conditions around it. Any deposit on a body would tend to insulate the body from the fire, and hence affect the heat flux to the body. These are second-order effects, however.

In addition, two other assumptions tend to make the model conservative: that the maximum value of ϵ always exists for the fire and that no air entrainment takes place. Hence the fire model should predict a higher heat flux than would exist in the actual case.

As long as deposition and convection are second-order effects, they can be accounted for by using an effective or corrected flame temperature in the basic fire-model equations (Eqs. 12 and 13). This correction is obtained from annular burn tests.

Determination of Adiabatic Flame Temperature

The product enthalpy based on equilibrium chemistry was calculated by the ACE computer code[5] as a function of temperature (Fig. 3). Complete results are given in the Appendix. These can be used to determine the adiabatic flame temperature since the heat of reaction at 77°F for a constant-pressure process is

$$\Delta H_{reaction} = H_{products} - H_{f\ reactant} \tag{18}$$

when no air is added to the reaction. This condition corresponds to the tests described below as well as to abort situations since the reaction zone for a solid propellant is very close to the gasifying surface and the propagation velocity is high.

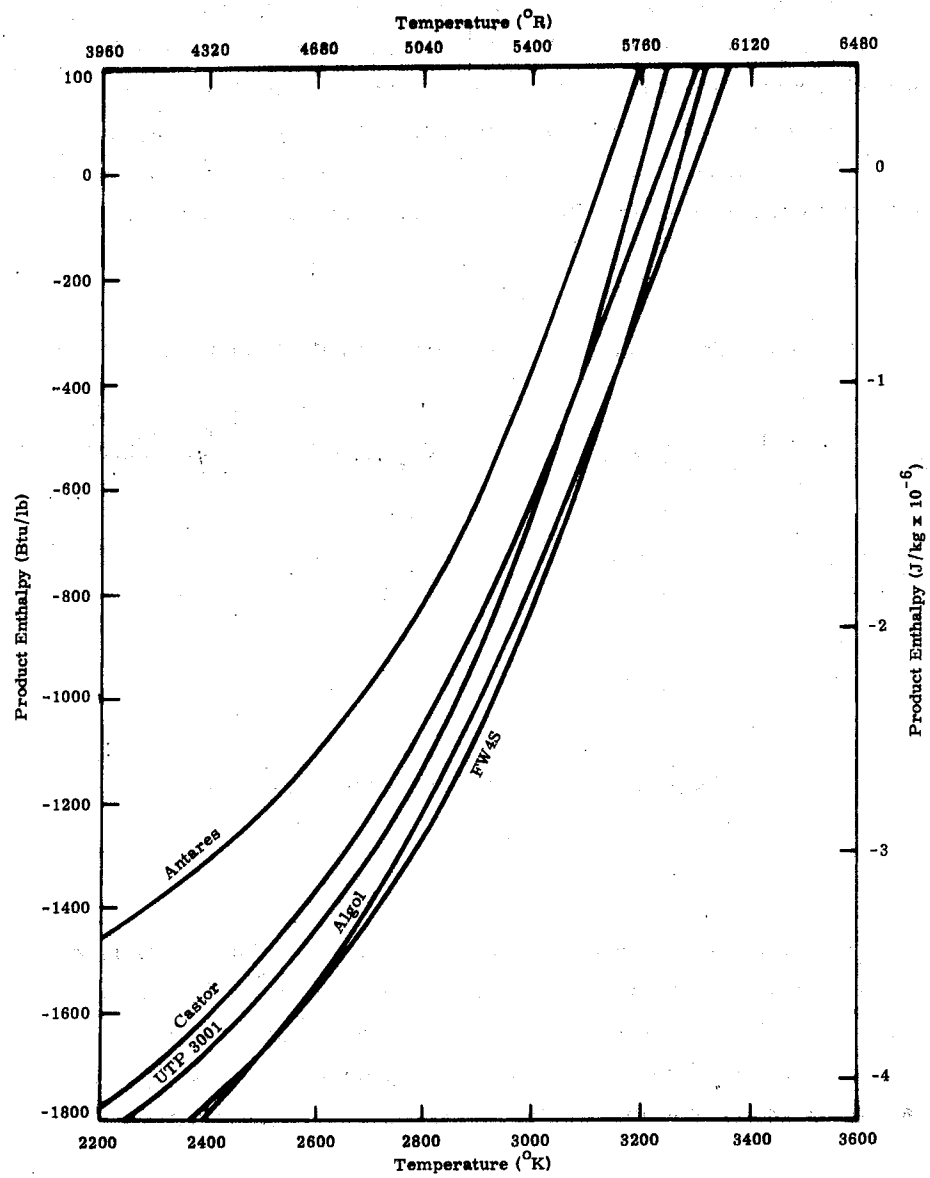

Figure 3. Product Enthalpies at 1 Atmosphere vs Temperature

In an adiabatic situation no energy is allowed to leave the system; hence

$$\Delta H_{reaction} = 0 \quad . \tag{19}$$

Then, for initial conditions at standard temperature and pressure

$$H_{products} = H_{f\ reactant}$$

where $H_{f\ reactant}$ can generally be obtained from the manufacturer. The adiabatic flame temperatures are given in Table I for the propellants tested. The estimates of $T_{adiabatic}$ were obtained by multiplying the adiabatic temperature at 1000 psi, reported by manufacturers, by the ratio of $T_{adiabatic}$ at 14.7 psia to $T_{adiabatic}$ at 1000 psia for Algol IIB. This technique was used because manufacturers do not usually report an adiabatic flame temperature at less than 1000 psi. These estimates are valid if it is assumed that (1) the reactant is incompressible, and (2) the only difference between burning at atmospheric pressure and at 1000 psia is the suppression of reactions at higher pressures (such as ionization or dissociation). Therefore, since this ratio is available for Algol IIB and since most propellants probably behave similarly, this method of approximating the atmospheric adiabatic flame temperature appears acceptable.

TABLE I

Adiabatic Flame Temperatures for Various Propellants at 1 Atmosphere

Propellant	$H_{f\ reactant}$ (Btu/lb)	$T_{adiabatic}$ (^{o}R)		
		Figure 3	Manufacturer	Estimated
Algol IIB (ANP-2872	-999	5230	5332	-
Castor II (TP-H7036)	-931	5150	-	5266
Antares II (X259-B3)	-821	5040	-	4532
FW4S (3096A)	NA	-	-	-
UTP 3001	~900	~5220	-	-

Burn Tests and Comparison of Results with Model

Test Setup

A summary of burn-test configurations, instrumentation, and burn rates is given in Table II. Detailed temperature records from these tests are given by Baker.[6] The ring type of calorimeter and the heat-flux gage used for these tests are shown in Figs. 4 and 5 respectively. Both gages are made of high-conductivity oxygen-free copper. The uses of the gages are illustrated in Figs. 6 and 7 for typical test setups. Note the method used for determining burn rate shown in Fig. 7.

TABLE II

Solid Propellant Burn Tests

Fuel Type	Configuration	Number of Tests	Instrumentation	Burn Rate (in. /sec)
UTP 3001	Annular cylinder, 7 in. dia. x 7 in. length, ≈15 lbs.	2	Ring type slug calorimeter Cylinder calorimeter Pyrometric photography	0.06
UTP 3001	Solid cylinder, 7 in. dia. x 7 in. length, ≈19 lbs.	2	Heat flux gage Pyrometric photography	
Algol IIB (ANP-2872)	Solid cylinder, one gallon, ≈15 lbs.	1	Heat flux gage Pyrometric photography	0.033
Algol IIB (ANP-2872)	Annular cylinder, one gallon, ≈15 lbs.	1	Ring type slug calorimeter Cylinder calorimeter	
Castor II (TP-H7036)	Solid cylinder, 6 in. dia. x 11 in. length, ≈19 lbs.	2	Heat flux gage Pyrometric photography	0.045
Castor II (TP-H7036)	Annular cylinder, 6 in. dia. x 11 in. length, ≈16 lbs.	1	Ring type slug calorimeter Cylinder calorimeter Pyrometric photography	
Antares II	8-inch cube with 2-inch diameter hole, ≈30 lbs.	1	Ring type slug calorimeter Pyrometric photography Cylinder calorimeter	0.029
FW4S (3096A)	Annular cylinder, 7 in. dia. x 10 in. length, ≈15 lbs.	1	Ring type slug calorimeter Cylinder calorimeter	0.050

To compare the model with experimental data, the propellant number is calculated based on the experimental burn rate and the theoretically determined adiabatic flame temperature at one atmosphere. These numbers are given in Table III.

TABLE III

Calculated Propellant Numbers at 1 Atmosphere

Propellant	P
Algol IIB	.166
Antares II	.176
Castor II	.387
FW4S	-
UTP 3001	.296

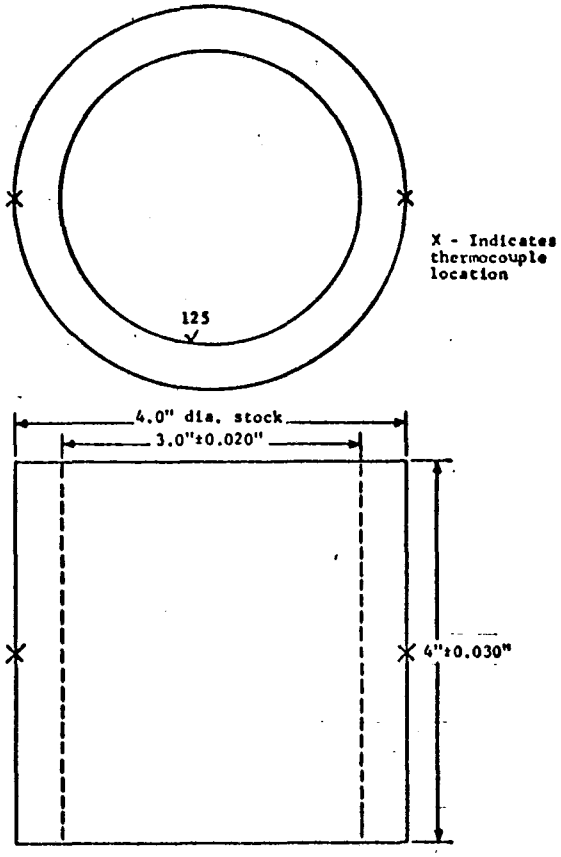

Figure 4. Ring Type Slug Calorimeter

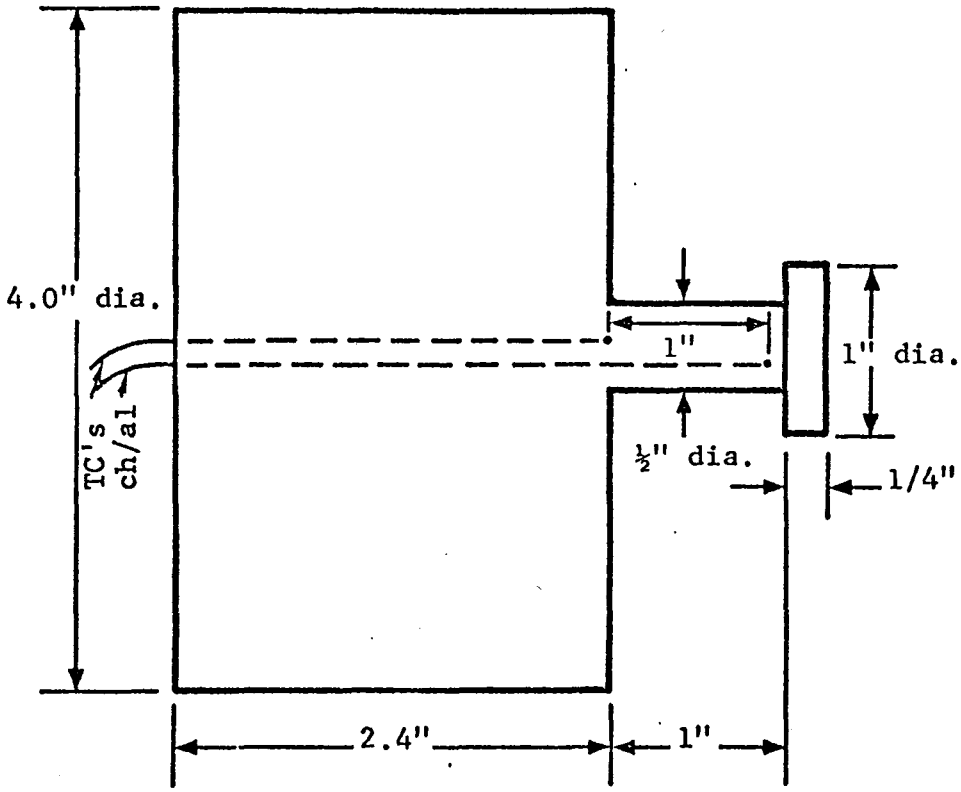

Figure 5. Heat Flux Gage

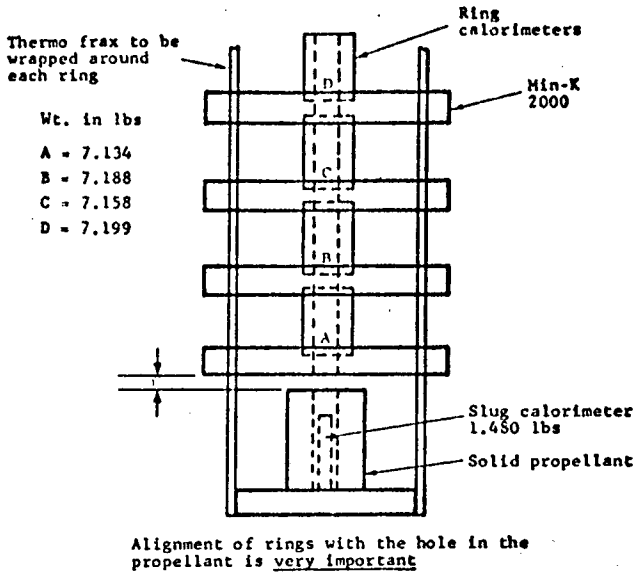

Figure 6. Typical Test Setup with Ring Calorimeters

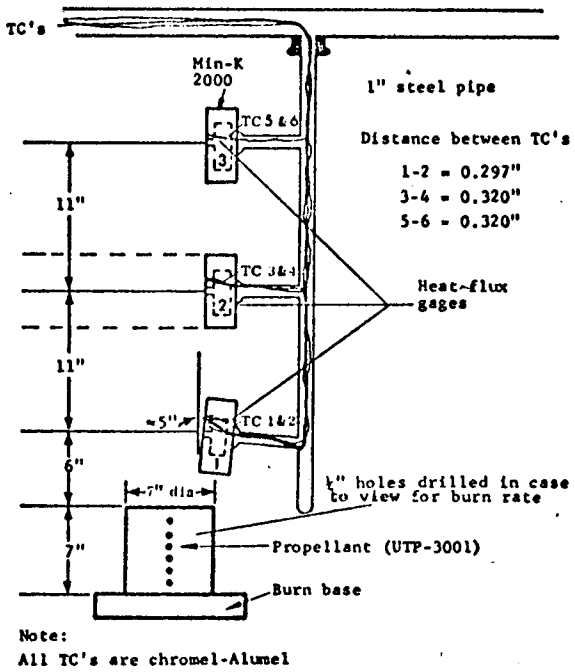

Figure 7. Typical Test Setup with Heat-Flux Gages

Annular Burn

Annular-burn data is given in Figs. 8-11 and is compared with the model for annular burns (Eqs. 16 and 17). The data in Fig. 8 compares well with the curve generated from the model. The two points at the intermediate values of X/L are above the curve and the two points at smaller values of X/L are below the curve. This may indicate that a reaction kinetics effect is present so that combustion is incomplete initially but is completed further up the plume, thus increasing the energy output at higher values of X/L.

Figures 9, 10, and 11 show the annular-burn results for Castor II, Algol IIB, and UTP 3001 solid propellants. No results were obtainable from the FW4S test, and no theoretical curve was calculable since $H_{f\ reactant}$ was unobtainable from the manufacturer. In these three cases the burn data consistently fall below (and for smaller values of X/L, well below) the theoretical curve. These results could indicate that the theoretical adiabatic flame temperatures are too high, or that the theoretical curves represent a worst-case situation based on the assumptions of no air entrainment and worst-case emissivity. There is some indication that it may be a combination of both, since movie coverage of the Algol IIB tests shows that it burned less violently than some of the other propellants with lower adiabatic flame temperatures.

Flat-Surface Burn

Figures 12-15 show the results of the thermal model for a flat-surface burn that would more closely approximate a real accident. Based on calorimeter data obtained from the annular burn at X/L = 0, these curves could be corrected for the apparently too high adiabatic flame temperature if it is assumed that the measured heat flux at X/L = 0 in the annular burn equals the measured heat flux at X/D = 0 in the flat-surface burn. The following relation would thus be obtained:

$$P_{actual} = P_{calculated} \left(\frac{q_{actual}}{q_{calculated}} \right)^{3/4} \tag{20}$$

where q_{actual} is the measured heat flux at X/L = 0 from the annular burn. The flat-burn model could then be modified:

$$q'_{max} = \frac{q_{actual}}{\left[1 + 2\,(P_{actual})\,\frac{X}{D} \right]^{4/3}}$$

for (21)

$$\frac{X}{D} \leq \frac{1}{4\,P_{actual}}$$

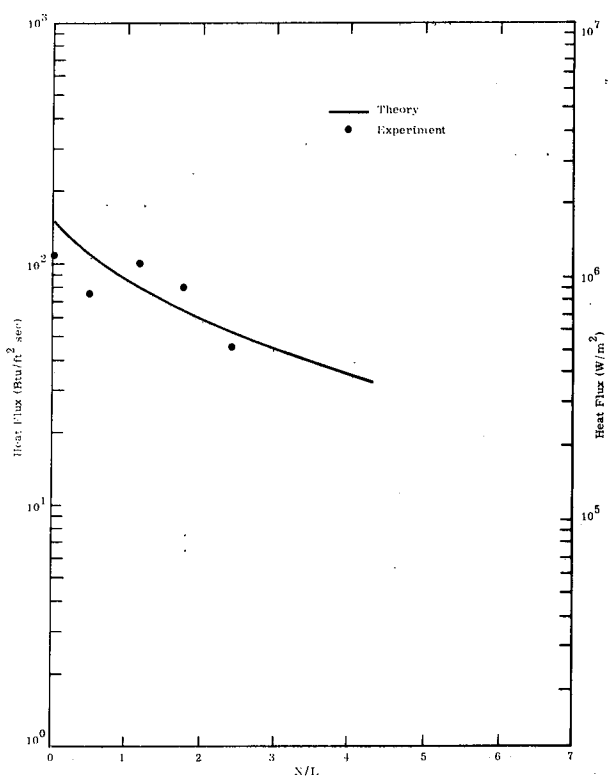

Figure 8. Incident Heat Flux for Annular Burn Antares Propellant

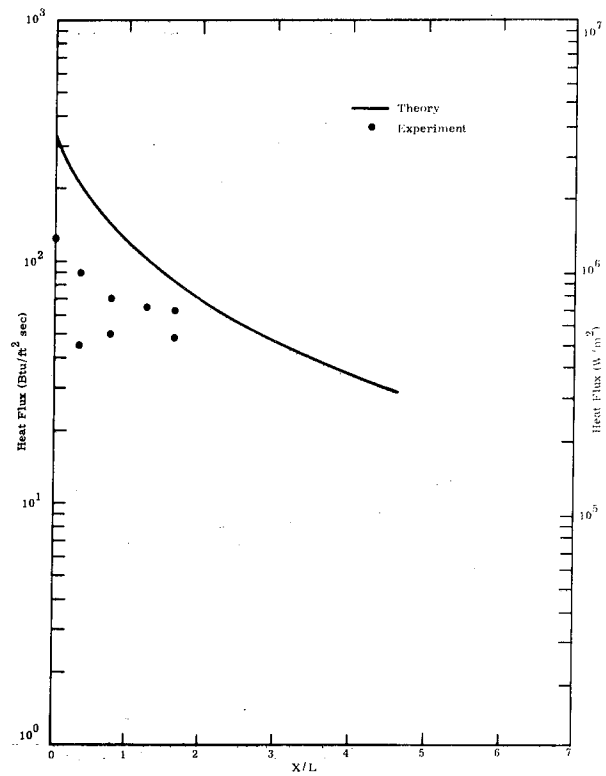

Figure 9. Incident Heat Flux for Annular Burn Castor Propellant

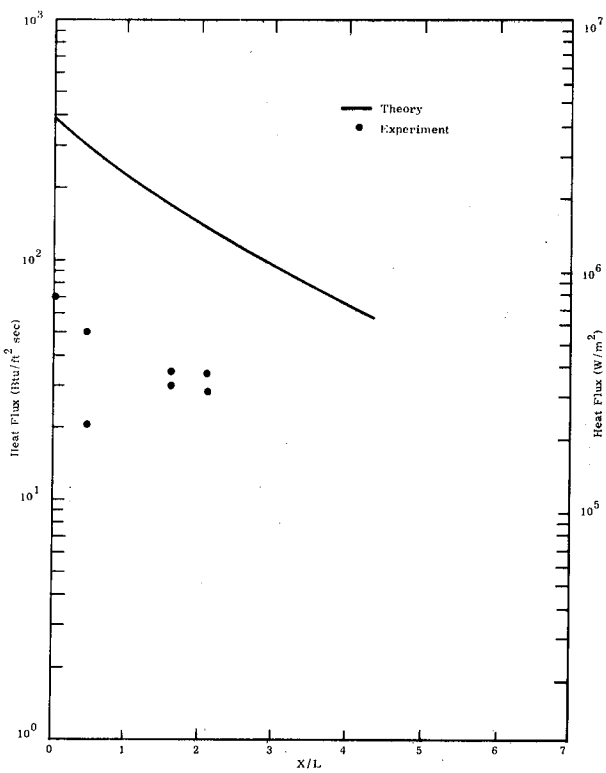

Figure 10. Incident Heat Flux for Annular Burn Algol IIB Propellant

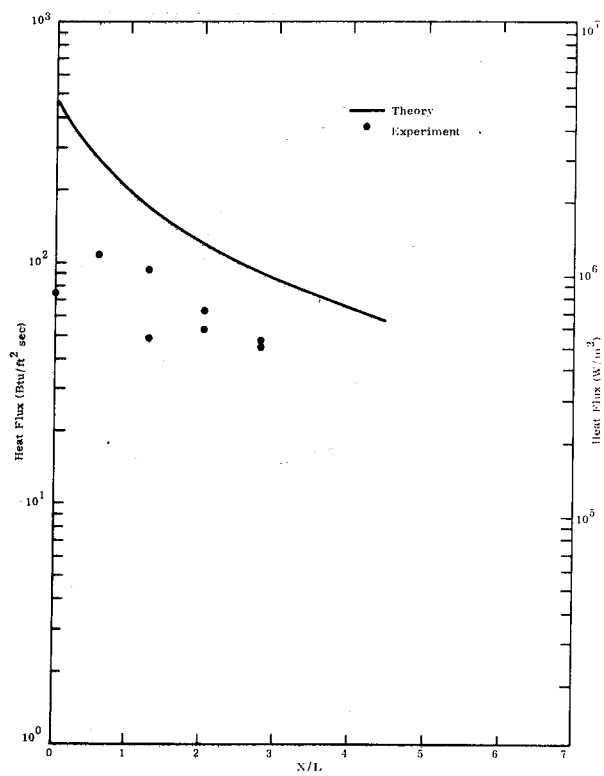

Figure 11. Incident Heat Flux for Annular Burn UTP 3001 Propellant

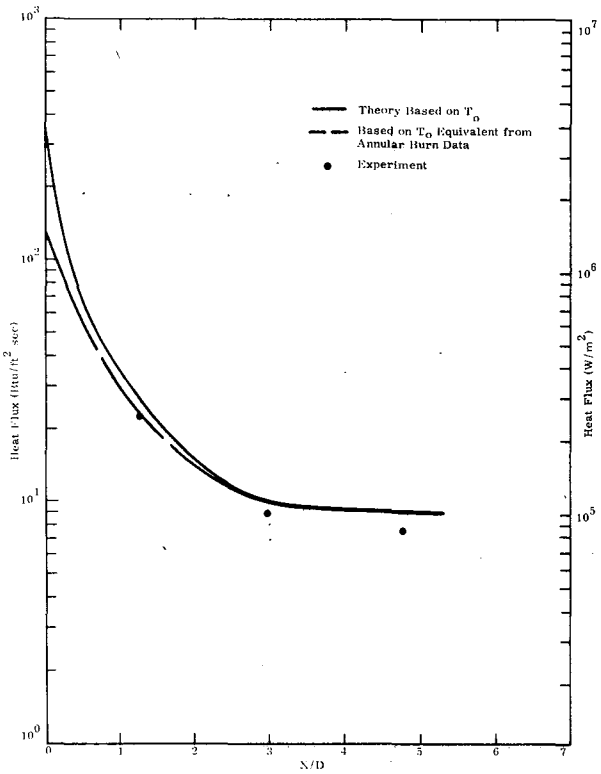

Figure 12. Incident Heat Flux for Flat Burn Castor Propellant

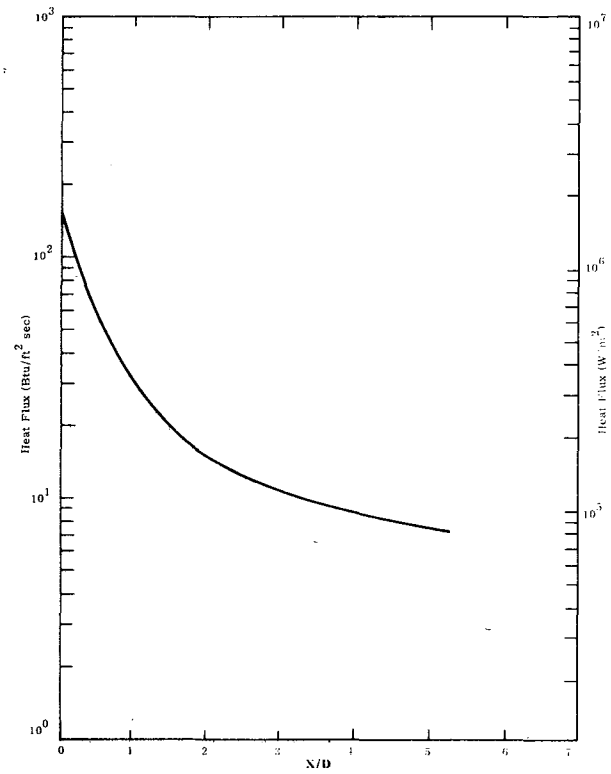

Figure 13. Incident Heat Flux for Flat Burn Antares Propellant

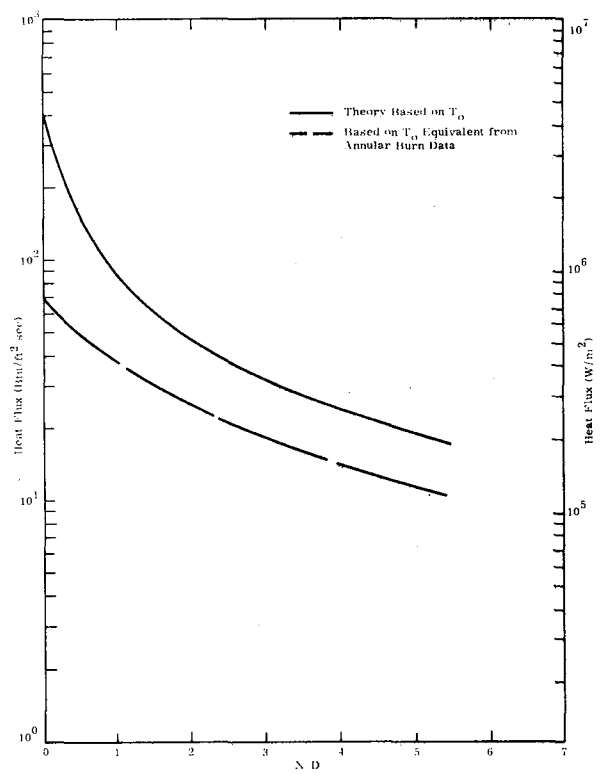

Figure 14. Incident Heat Flux for Flat Burn Algol IIB Propellant

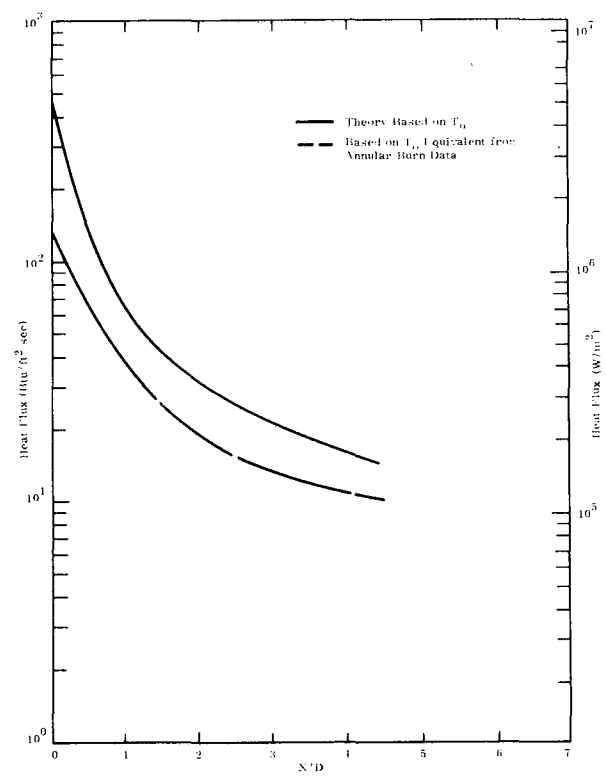

Figure 15. Incident Heat Flux for Flat Burn UTP 3001 Propellant

and

$$q'_{max} = \frac{q_{actual}}{(4)^{7/3} P_{actual} \frac{X}{D}}$$

for (22)

$$\frac{X}{D} \geq \frac{1}{4 P_{actual}}$$

The dashed curves based on Eqs. 21 and 22 would then represent a more realistic heat flux, while the curves based on Eqs. 12 and 13 would represent a theoretical upper limit.

Data obtained from the Castor II propellant agrees with the corrected theoretical curves (Fig. 12). This is also the only data that now exists for flat-surface burns. Figures 13, 14, and 15 show theoretical curves for Antares, Algol IIB, and UTP 3001 flat burns. Figures 14 and 15 also show the dashed curves that are based on a corrected theoretical flame temperature from the annular-burn tests.

Discussion of the Discrepancy in Adiabatic Flame Temperatures

The results given in the previous section show that even though the Algol IIB had the highest calculated adiabatic flame temperature, the actual burn data shows that it had the lowest heat flux. This appears to be related to the ratio of aluminum to oxygen in the constituents of the propellant. These ratios are given in Table IV. Note that the higher the ratio, the greater the deviation from the theoretical curve, especially at small values of X/L. The ratio for the Antares II propellant is smallest and the data agrees very well with the theoretical curve.

TABLE IV

Ratio of Aluminum to Oxygen in the Constituents of the Propellant

Propellant	Al/Oxygen
Algol IIB	.4996
Castor II	.3576
Antares II	.0527
FW4S	.4208
UTP 3001	.4149

The following explanation for the low heat flux is hypothesized. The energy released per mole of oxygen for the reaction

$$4\ Al + 3\ O_2 \longrightarrow 2\ Al_2\ O_3$$

is more than 2.5 times that of the reaction

$$C + O_2 \longrightarrow CO_2$$

Thus if the oxygen in the propellant reacted preferentially with the carbon rather than with the aluminum when the amount of oxygen in the system is insufficient for complete reaction of the aluminum, the enthalpy would be greater than in a system where aluminum and carbon oxidation are governed by equilibrium chemistry. Therefore the enthalpy curves of Fig. 3 should be shifted upward for all the propellants except Antares II. Hence the true maximum temperature would be lower than the theoretical adiabatic flame temperature under these conditions of nonequilibrium.

Two observations tend to support the hypothesis. First, it was noticed in films of the experimental burns that beads of liquid form on the burning surface, dance about, coalesce, and then are blown out as a shower of sparks. Examination of the test site after a burn showed a large quantity of free aluminum on the heat gages and on the ground, particularly after the Castor II and Algol IIB fires. The chemical species table based on equilibrium calculations for these propellant products shows only minute amounts of free aluminum in the temperature range 4500 to 5400°R.

Second, bomb calorimeter tests show that although Algol IIB has the lowest heat of explosion, it has the highest heat of combustion. For the heat-of-explosion tests no oxygen was added. This resulted in the aluminum being unburned and in small heat being released. However, for the heat-of-combustion tests excess oxygen was present, allowing complete combustion of aluminum, together with high heat release.

Conclusions

Presently available data agrees well with the thermal model. Figures 12-15 give the best current estimates of the incident heat flux for both maximum and expected values. These are cold-wall heat rates and a hot-wall correction will have to be used in analyses based on the heat rates given in this report. Outside the flame, the heat flux can be estimated from the thermal model with the use of view factors. The maximum heat flux, however, occurs in the flame near the burning surface.

Recommendations

Future work should include design of instrumentation that would give both maximum flame temperature and maximum heat flux. This information would be useful in estimating the degree of nonequilibrium for the reaction products. The relative amounts of free aluminum from the different propellant burns should be checked to determine whether there is a correlation with propellant type. The possibility of extending this existing model to include the effects of the aluminum-to-oxygen ratio should be examined. Techniques for correcting instrument readings when the instruments become coated with combustion products should also be developed since some types of propellants deposit great quantities of residue on the gages.

References

1. L. J. Van Nice and H. J. Carpenter, "Thermal Radiation from Saturn Fireballs," TRW Systems, Redondo Beach, California, NAS 9-4810, December 1965.

2. F. D. Kite and B. E. Bader, "Pad-Abort Thermal Flux Model for Liquid Rocket Propellants," Sandia Laboratories, Albuquerque, N. M., SC-RR-66-577, November 1966.

3. B. E. Bader, A. B. Donaldson, and H. C. Hardee, "Liquid-Propellant Rocket Abort Fire Model," Journal of Spacecraft and Rockets, Vol. 8, pp. 1216-1219, December 1971.

4. H. C. Hardee and D. O. Lee, "Thermal Hazard from Propane Fireballs," Transportation Planning and Technology, Vol. 2, pp. 121-128, 1973.

5. C. A. Powars and R. Kendall, "Aerotherm Chemical Equilibrium (ACE) Computer Program," Aerotherm/Acurex Corporation, Mountain View, Calif., May 1969.

6. F. L. Baker, "Solid Propellant Burn Tests," SC-DR-71-0084, Sandia Laboratories, Albuquerque, N. M., March 1971.

APPENDIX

TABLE A-I

System Compositions (Mass Fraction)

Fuel Mixture	Antares	Algol	Castor	FW4S	UTP 3001
Hydrogen	0.02827	0.04027	0.03968	0.03774	0.03884
Carbon	0.23430	0.12795	0.13080	0.12371	0.11786
Nitrogen	0.12885	0.07716	0.08704	0.08348	0.08612
Oxygen	0.55057	0.38052	0.39095	0.38975	0.38543
Aluminum	0.02900	0.19010	0.13981	0.16400	0.15992
Chlorine	-	0.18400	0.21172	0.20132	0.21122
Lead	0.02901	-	-	-	-
Sulfur	-	-	-	-	0.00061

TABLE A-II

System Enthalpies* (Btu/lb)

Temperature (°R)	Gas	Condensed	Composite
	Antares		
900	-3592.90	-2075.31	-3319.36
1800	-2241.49	-4395.12	-2421.70
2700	-1771.83	-6467.64	-2029.14
3600	-1398.51	-6182.78	-1660.67
4500	- 970.78	-5384.70	-1212.31
5400	- 113.33	-5079.07	- 373.85
6300	2066.19	---	2066.19
	Algol		
900	-2683.79	-5967.71	-4062.03
1800	-1103.70	-6739.26	-3127.97
2700	- 602.75	-6467.64	-2709.40
3600	- 165.83	-6182.78	-2326.64
4500	368.80	-5384.70	-1678.41
5400	1286.66	-5079.07	- 782.24
6300	3051.80	-4773.45	1918.11

*Referenced to JANAF base state: 1 atm and 298 K.

TABLE A-II (cont)

Temperature (°R)	Gas	Condensed	Composite
	Castor		
900	-2762.08	-5674.19	-3706.74
1800	-1438.02	-6739.26	-2838.46
2700	-1011.15	-6467.64	-2452.61
3600	- 602.90	-6182.78	-2076.79
4500	- 100.07	-5384.70	-1489.10
5400	840.03	-5079.07	- 615.71
6300	2815.27	-4773.45	2129.04
	FW4S		
900	-2726.33	-5874.75	-3884.06
1800	-1372.71	-6739.26	-3035.70
2700	- 941.13	-6467.64	-2653.69
3600	- 531.16	-6182.78	-2282.30
4500	- 26.03	-5384.70	-1678.76
5400	906.80	-5079.07	- 832.42
6300	2834.83	-4773.45	1787.13
	UTP 3001		
540	-4567.30	-4231.34	-4335.64
900	-2684.82	-5962.95	-3843.12
1800	-1399.26	-6739.26	-3012.85
2700	-970.82	-6467.64	-2631.80
3600	-559.45	-6182.78	-2258.48
4500	-50.10	-5384.70	-1654.59
5400	898.72	-5079.07	-795.37
6300	2874.00	-4773.45	1879.21

*Referenced to JANAF base state: 1 atm and 298 K.

TABLE A-III

Dominant Species with Antares (Mole Fraction of Gas)

900°R		1800°R		2700°R		3600°R		4500°R		5400°R		6300°R	
H_2O	0.423060	CO	0.286830	CO	0.354770	Co	0.382267	CO	0.393292	CO	0.392658	CO	0.359652
CO_2	0.372712	H_2	0.240823	H_2O	0.192371	H_2O	0.219746	H_2O	0.227756	H_2O	0.187691	H	0.178533
N_2	0.163844	CO_2	0.224794	H_2	0.174051	H_2	0.146194	H_2	0.130099	H_2	0.116069	H_2	0.092247
CH_4	0.036153	H_2O	0.125597	CO_2	0.154955	CO_2	0.127276	N_2	0.119293	N_2	0.111827	N_2	0.088203
H_2	0.004174	N_2	0.120869	N_2	0.120185	N_2	0.120141	CO_2	0.113098	CO_2	0.087969	O	0.068955
NH_3	0.000032	CH_4	0.001047	Pb	0.003645	Pb	0.003555	H	0.009029	H	0.053551	H_2O	0.067026
CO	0.000025	NH_3	0.000023	Al_2O_3*	0.014043	H	0.000620	Pb	0.003288	OH	0.029022	OH	0.060787
C*	0.286065	Pb	0.000016			PbO	0.000095	OH	0.003279	O	0.008241	CO_2	0.032668
Al_2O_3*	0.019147	Al_2O_3*	0.014125			OH	0.000093	PbO	0.000337	O_2	0.005378	O_2	0.019838
Pb*	0.004988	Pb*	0.003664			Al_2O_3*	0.014038	NO	0.000214	NO	0.002994	NO	0.008532
								O	0.00015U	Pb	0.002860	Al	0.005823
								O_2	0.000109	AlO_2H	0.000774	AlO	0.004848
								AlO_2H	0.000033	PbO	0.000579	AlO_2H	0.004159
								Al_2O_3*	0.013932	AlOH	0.000147	AlO_2	0.002815
										AlO_2	0.000093	Pb	0.002439
										AlO	0.000069	AlOH	0.001944
										Al	0.000040	Al_2O	0.000958
										HCO	0.000014	PbO	0.000368
										PbH	0.000011	AlH	0.000068
										Al_2O_3*	0.012678	N	0.000065
												Al_2O_2	0.000022
												HCO	0.000019

*Indicates a solid or liquid species; others are gaseous.

TABLE A-IV

Dominant Species with Algol (Mole Fraction of Gas)

900°R		1800°R		2700°R		3600°R		4500°R		5400°R		6300°R	
H_2O	0.410242	H_2	0.423141	H_2	0.426600	H_2	0.420552	H_2	0.407928	H_2	0.345341	H	0.242992
HCl	0.222317	CO	0.249839	CO	0.281367	CO	0.286554	CO	0.285457	CO	0.268148	CO	0.211692
CH_4	0.162651	HCl	0.148165	HCl	0.144250	HCl	0.143802	HCl	0.136308	HCl	0.099273	H_2	0.185237
N_2	0.117943	N_2	0.078610	N_2	0.076554	N_2	0.076504	N_2	0.075730	H	0.092371	H_2O	0.059020
CO_2	0.077900	H_2O	0.045923	H_2O	0.056484	H_2O	0.061865	H_2O	0.064927	H_2O	0.072443	N_2	0.055404
H_2	0.008852	CO_2	0.040745	CO_2	0.014722	CO_2	0.009337	H	0.015987	N_2	0.071192	OH	0.037772
NH_3	0.000083	CH_4	0.013532	H	0.000011	H	0.001051	CO_2	0.007463	Cl	0.018205	HCl	0.037281
CO	0.000011	NH_3	0.000043	Al_2O_3*	0.097921	Cl	0.000271	Cl	0.003808	AlCl	0.010614	Cl	0.033961
C*	0.215756	Al_2O_3*	0.100576			$AlCl_2$	0.000030	AlCl	0.000802	CO_2	0.007793	O	0.030237
Al_2O_3*	0.150910					OH	0.000015	$AlCl_2$	0.000784	OH	0.006494	AlCl	0.027231
						Al_2O_3*	0.097835	OH	0.000528	$AlCl_2$	0.002116	Al	0.021510
								AlOCl	0.000159	AlOCl	0.002072	CO_2	0.008432
								AlOH	0.000029	O	0.001069	AlO	0.007854
								$AlCl_3$	0.000022	Al	0.000854	AlOCl	0.006632
								AlO_2H	0.000018	AlOH	0.000703	Al_2O	0.005733
								NO	0.000016	AlO_2H	0.000481	AlOH	0.004464
								O	0.000014	NO	0.000310	AlO_2H	0.004187
								Al_2O_3*	0.095965	AlO	0.000193	O_2	0.003815
										Al_2O	0.000132	NO	0.002965
										O_2	0.000090	AlO_2	0.001999
										AlO_2	0.000033	$AlCl_2$	0.001058
										AlH	0.000029	AlH	0.000354
										HCO	0.000016	Al_2O_2	0.000056
										$AlCl_3$	0.000013	N	0.000052
										Al_2O_3*	0.082575	HCO	0.000016
												ClO	0.000016
												Al_2O_3*	0.029364

*Indicates a solid or liquid species; others are gaseous.

TABLE A-V

Dominant Species with Castor (Mole Fraction of Gas)

900°R		1800°R		2700°R		3600°R		4500°R		5400°R		6300°R	
H_2O	0.414147	H_2	0.365166	H_2	0.334909	H_2	0.322268	H_2	0.310400	H_2	0.270266	H	0.236022
HCl	0.230989	CO	0.218324	CO	0.260040	CO	0.272029	CO	0.274242	CO	0.260642	CO	0.209124
N_2	0.120147	HCl	0.164203	HCl	0.162866	HCl	0.162382	HCl	0.155233	H_2O	0.123762	H_2	0.161219
CO_2	0.115166	H_2O	0.085748	H_2O	0.120466	H_2O	0.132531	H_2O	0.135619	HCl	0.118631	H_2O	0.068774
CH_4	0.112124	N_2	0.085413	N_2	0.084736	N_2	0.084682	N_2	0.083838	H	0.081716	N_2	0.060740
H_2	0.007350	CO_2	0.077039	CO_2	0.036963	CO_2	0.024780	CO_2	0.019682	N_2	0.078726	OH	0.047180
NH_3	0.000063	CH_4	0.004070	H	0.000010	H	0.000920	H	0.013946	Cl	0.024591	HCl	0.044771
CO	0.000014	NH_3	0.000036	Al_2O_3*	0.070664	Cl	0.000350	Cl	0.004972	CO_2	0.016536	Cl	0.043716
C*	0.193917	Al_2O_3*	0.071242			OH	0.000038	OH	0.001264	OH	0.012541	O	0.040483
Al_2O_3*	0.100219					$AlCl_2$	0.000011	$AlCl_2$	0.000294	AlCl	0.004445	AlCl	0.022627
						Al_2O_3*	0.070611	AlCl	0.000230	O	0.002334	Al	0.013885
								AlOCl	0.000126	AlOCl	0.001894	CO_2	0.011152
								NO	0.000045	$AlCl_2$	0.001197	AlCl	0.007379
								O	0.000038	NO	0.000711	O_2	0.006838
								AlO_2H	0.000025	AlO_2H	0.000628	AlO	0.006788
								AlOH	0.000015	O_2	0.000431	AlO_2H	0.004520
								$AlCl_3$	0.000011	AlOH	0.000421	NO	0.004157
								Al_2O_3*	0.069582	Al	0.000265	AlOH	0.003599
										AlO	0.000130	Al_2O	0.003198
										AlO_2	0.000049	AlO_2	0.002313
										Al_2O	0.000028	$AlCl_2$	0.001132
										HCO	0.000014	AlH	0.000213
										Al_2O_3*	0.061398	N	0.000054
												Al_2O_2	0.000042
												ClO	0.000028
												HCO	0.000015
												Al_2O_3*	0.017941

*Indicates a solid or liquid species; others are gaseous.

TABLE A-VI

Dominant Species with FW4S (Mole Fraction of Gas)

900°R		1800°R		2700°R		3600°R		4500°R		5400°R		6300°R	
H_2O	0.410710	H_2	0.372592	H_2	0.346679	H_2	0.335195	H_2	0.323407	H_2	0.280353	H	0.237996
HCl	0.233572	CO	0.223438	CO	0.262916	CO	0.273720	CO	0.275349	CO	0.261158	CO	0.208812
N_2	0.122539	HCl	0.164583	HCl	0.162984	HCl	0.162501	HCl	0.155277	HCl	0.118150	H_2	0.163928
CH_4	0.117458	N_2	0.086350	H_2O	0.109156	H_2O	0.120054	H_2O	0.123008	H_2O	0.114238	H_2O	0.066835
CO_2	0.108119	H_2O	0.077915	N_2	0.085531	N_2	0.085476	N_2	0.084624	H	0.083227	N_2	0.061466
H_2	0.007523	CO_2	0.070213	CO_2	0.032714	CO_2	0.021716	CO_2	0.017203	N_2	0.079507	OH	0.045469
NH_3	0.000066	CH_4	0.004870	H	0.000010	H	0.000938	H	0.014235	Cl	0.024047	HCl	0.044392
CO	0.000013	NH_3	0.000037	Al_2O_3*	0.087236	Cl	0.000343	Cl	0.004872	CO_2	0.014744	Cl	0.042986
C*	0.198063	Al_2O_3*	0.088089			OH	0.000033	OH	0.001123	OH	0.011366	O	0.038692
Al_2O_3*	0.125014					$AlCl_2$	0.000013	$AlCl_2$	0.000347	AlCl	0.005179	AlCl	0.023812
						Al_2O_3*	0.087170	AlCl	0.000278	O	0.002077	Al	0.014860
								AlOCl	0.000132	AlOCl	0.001964	CO_2	0.010643
								NO	0.000039	$AlCl_2$	0.001364	AlOCl	0.007421
								O	0.000033	NO	0.000636	AlO	0.006943
								AlO_2H	0.000024	AlO_2H	0.000603	O_2	0.006246
								AlOH	0.000017	AlOH	0.000455	AlO_2H	0.004455
								$AlCl_3$	0.000013	O_2	0.000341	NO	0.003997
								Al_2O_3*	0.085924	Al	0.000316	Al_2H	0.003712
										AlO	0.000138	Al_2O	0.003501
										AlO_2	0.000046	Al_2O	0.002262
										Al_2O	0.000035	$AlCl_2$	0.001172
										HCO	0.000014	AlH	0.000230
										$AlCl_3$	0.000011	N	0.000055
										Al_2O_3*	0.076341	Al_2O_2	0.000044
												ClO	0.000026
												HCO	0.000015
												Al_2O_3*	0.028779

*Indicates a solid or liquid species; others are gaseous.

TABLE A-VII

Dominant Species with UTP 3001 (Mole Fraction of Gas)

540°R		900°R		1800°R		2700°R		3600°F		4500°R		5400°F		6300°R	
H_2O	0.630327	H_2O	0.405384	H_2	0.372091	H_2	0.343516	H_2	0.331770	H_2	0.320395	H_2	0.278812	H	0.238915
CO_2	0.352645	HCl	0.239466	CO	0.205599	CO	0.245524	CO	0.256681	CO	0.253584	CO	0.245362	CO	0.196062
N_2	0.008374	N_2	0.123530	HCl	0.170947	HCl	0.169575	HCl	0.169061	HCl	0.161557	HCl	0.123319	H_2	0.165196
CH_4	0.006976	CH_4	0.120398	N_2	0.086190	H_2O	0.119555	H_2O	0.130754	H_2O	0.133365	H_2O	0.122403	H_2O	0.069497
H_2S	0.001672	CO_2	0.102761	H_2O	0.086637	N_2	0.087501	N_2	0.087438	N_2	0.086531	H	0.082998	N_2	0.062545
NH_4Cl*	0.523531	H_2	0.007616	CO_2	0.071937	CO_2	0.033768	CO_2	0.022408	CO_2	0.017681	N_2	0.081198	OH	0.047098
C*	0.502656	H_2S	0.000765	CH_4	0.004014	H_2S	0.000526	H	0.000934	H	0.014169	Cl	0.025168	HCl	0.046551
Al_2O_3*	0.260430	NH_3	0.000068	H_2S	0.000536	COS	0.000013	H_2S	0.000424	Cl	0.005093	CO_2	0.014924	Cl	0.044904
		CO	0.000013	NH_3	0.000038	H	0.000010	Cl	0.000359	OH	0.001224	OH	0.012212	O	0.039924
		C*	0.171238	Al_2O_3*	0.085038	Al_2O_3*	0.084358	SH	0.000064	$AlCl_2$	0.000331	AlCl	0.004847	AlCl	0.023732
		Al_2O_3*	0.119122					OH	0.000037	AlCl	0.000254	O	0.002237	Al	0.014178
								SO	0.000014	SH	0.000140	AlOCl	0.001980	CO_2	0.010311
								SO_2	0.000012	AlOCl	0.000132	$AlCl_2$	0.001336	AlOCl	0.007632
								$AlCl_2$	0.000012	SO	0.000129	NO	0.000693	AlO	0.006835
								COS	0.000012	H_2S	0.000118	AlO_2H	0.000625	O_2	0.006650
								Al_2O_3*	0.084287	S	0.000073	AlOH	0.000437	AlO_2H	0.004543
										SO_2	0.000065	O_2	0.000396	NO	0.004160
										NO	0.000043	Al	0.000282	AlOH	0.003668
										O	0.000036	SO	0.000202	Al_2O	0.003289
										AlO_2H	0.000025	S	0.000135	AlO_2	0.002297
										AlOH	0.000016	AlO	0.000133	$AlCl_2$	0.001220
										$AlCl_3$	0.000013	SH	0.000077	AlH	0.000221
										Al_2O_3*	0.083056	SO_2	0.000072	SO	0.000176
												AlO_2	0.000048	S	0.000145
												Al_2O	0.000030	N	0.000055
												H_2S	0.000016	SO_2	0.000046
												HCO	0.000013	Al_2O_2	0.000043
												$AlCl_3$	0.000011	SH	0.000028
												Al_2O_3*	0.073733	ClO	0.000028
														HCO	0.000014
														Al_2O_3*	0.026834

*Indicates a solid or liquid species; others are gaseous.

TABLE A-III

Molecular Weights*

Species	Molecular Weight	Species	Molecular Weight
Al	26.98	ClO	51.4524
AlCl	62.433	H	1.00797
$AlCl_2$	97.886	HCO	29.01837
$AlCl_3$	133.339	HCl	36.46097
AlH	27.98797	H_2	2.01594
AlO	42.9794	H_2O	18.01534
AlOCl	78.4324	N	14.007
AlOH	43.98737	NH_3	17.03091
AlO_2	58.9788	NO	30.0064
AlO_2H	59.98677	N_2	28.014
Al_2O	69.9594	O	15.9994
Al_2O_2	85.9588	OH	17.00737
Al_2O_3*	101.9582	O_2	31.9988
C*	12.011	Pb	207.19
CH_4	16.04288	Pb*	207.19
CO	28.0104	PbH	208.19797
CO_2	44.0098	PbO	223.1894
Cl	35.453		

*A revised set of molecular weights was determined by the IUPAC (see Chemical and Engineering News 48, No. 4, Jan. 26, 1970, pp. 38-39) but these values are retained here for consistency.

TABLE A-IX

System Molecular Weights

Temperature (°R)	Gas	Condensed	Composite
	Antares		
900	29.2042	20.7014	35.6257
1800	24.0821	123.6316	26.2813
2700	24.6984	101.9582	26.1302
3600	24.6897	101.9582	26.1210
4500	24.5391	101.9582	25.9596
5400	23.3466	101.9582	24.6393
6300	20.1126	--	20.1126
	Algol		
900	24.8579	49.0309	42.8359
1800	18.2939	101.9582	28.5484
2700	17.8111	101.9582	27.7949
3600	17.8014	101.9582	27.7764
4500	17.7137	101.9582	27.4981
5400	17.4856	101.9582	25.9049
6300	17.6712	101.9582	20.6651
	Castor		
900	26.1324	42.6580	38.6796
1800	20.2324	101.9582	27.4962
2700	20.0683	101.9582	27.2731
3600	20.0561	101.9582	27.2554
4500	19.8965	101.9582	26.9909
5400	19.1938	101.9582	25.4539
6300	18.3996	101.9582	20.2288

TABLE A-IX (cont)

Temperature (°R)	Gas	Condensed	Composite
	FW4S		
900	26.0075	46.8158	41.1326
1800	20.0021	101.9582	28.9835
2700	19.8084	101.9582	28.7028
3600	19.7964	101.9582	28.6841
4500	19.6441	101.9582	28.4047
5400	19.0052	101.9582	26.7888
6300	18.3741	101.9582	21.3084
	UTP 3001		
540	27.2789	47.0964	87.8739
900	25.9918	48.9124	40.1940
1800	20.0232	101.9582	28.6935
2700	19.8629	101.9582	28.4638
3600	19.8494	101.9582	28.4431
4500	19.6868	101.9582	28.1551
5400	19.0093	101.9582	26.5269
6300	18.2968	101.9582	21.0328

DISTRIBUTION:
Capt. Dayton Silver
SAMSO. MNNPX
Norton AFB, CA 92409

J. Koury
Air Force Rocket Propulsion Lab.
AFRPL/MKMB
Edwards Air Force Base
Edwards, CA 93523

W. Hubbell
Mail Station L 125
LLL
Livermore, CA 94550

1200 W. A. Gardner
1500 R. L. Peurifoy, Jr.
1540 T. B. Lane
1543 H. C. Hardee (25)
1543 D. W. Larson
1543 D. O. Lee (25)
1560 E. E. Ives
1561 W. C. Hines
1650 W. L. Stevens
1700 O. E. Jones
2510 D. H. Anderson
2515 E. A. Kjeldgaard
2515 A. B. Donaldson (25)
4700 D. B. Shuster
4734 R. D. Klett
5131 J. E. Kennedy
5628 S. McAlees, Jr., Attn: M. L. Carnicom
5700 J. H. Scott
8110 A. N. Blackwell
8345 F. J. Murar
8266 E. A. Aas (2)
3141 L. S. Ostrander (5)
3151 W. L. Garner (3)
for ERDA/TIC (Unlimited Release)
ERDA/TIC (25)
(R. P. Campbell, 3171-1)